



Molecular Gas in Three $z \sim 7$ Quasar Host Galaxies

Bram P. Venemans¹ , Fabian Walter¹ , Roberto Decarli¹ , Carl Ferkinhoff² , Axel Weiß³ , Joseph R. Findlay⁴, Richard G. McMahon^{5,6} , Will J. Sutherland⁷, and Rowin Meijerink⁸

¹ Max-Planck Institute for Astronomy, Königstuhl 17, D-69117 Heidelberg, Germany; venemans@mpia.de

² Department of Physics, Winona State University, Winona, MN 55987, USA

³ Max-Planck-Institut für Radioastronomie, Auf dem Hügel 69, D-53121 Bonn, Germany

⁴ Department of Physics & Astronomy, University of Wyoming, Laramie, WY 82070, USA

⁵ Institute of Astronomy, University of Cambridge, Madingley Road, Cambridge CB3 0HA, UK

⁶ Kavli Institute for Cosmology, University of Cambridge, Madingley Road, Cambridge CB3 0HA, UK

⁷ Astronomy Unit, Queen Mary University of London, London, E1 4NS, UK

⁸ Leiden Observatory, Leiden University, P.O. box 9513, NL-2300 RA Leiden, The Netherlands

Received 2017 April 28; revised 2017 July 4; accepted 2017 July 17; published 2017 August 22

Abstract

We present ALMA band 3 observations of the CO(6–5), CO(7–6), and [C I] 369 μm emission lines in three of the highest-redshift quasar host galaxies at $6.6 < z < 6.9$. These measurements constitute the highest-redshift CO detections to date. The target quasars have previously been detected in [C II] 158 μm emission and the underlying FIR dust continuum. We detect (spatially unresolved, at a resolution of $>2''$, or $\gtrsim 14$ kpc) CO emission in all three quasar hosts. In two sources, we detect the continuum emission around 400 μm (rest-frame), and in one source we detect [C I] at low significance. We derive molecular gas reservoirs of $(1\text{--}3) \times 10^{10} M_\odot$ in the quasar hosts, i.e., approximately only 10 times the mass of their central supermassive black holes. The extrapolated [C II]-to-CO (1–0) luminosity ratio is 2500–4200, consistent with measurements in galaxies at lower redshift. The detection of the [C I] line in one quasar host galaxy and the limit on the [C I] emission in the other two hosts enables a first characterization of the physical properties of the interstellar medium in $z \sim 7$ quasar hosts. In the sources, the derived global CO/[C II]/[C I] line ratios are consistent with expectations from photodissociation regions, but not X-ray-dominated regions. This suggests that quantities derived from the molecular gas and dust emission are related to ongoing star-formation activity in the quasar hosts, providing further evidence that the quasar hosts studied here harbor intense starbursts in addition to their active nucleus.

Key words: cosmology: observations – galaxies: active – galaxies: high-redshift – galaxies: ISM

1. Introduction

Quasars are the most luminous, non-transient objects in the universe, and can be observed out to very high redshifts (e.g., Fan et al. 2006; Mortlock et al. 2011; Venemans et al. 2013; Bañados et al. 2016). In the case of quasars at $z > 6$ (the age of the universe: < 1 Gyr), optical and near-infrared (NIR) observations trace the (rest-frame) UV emission of the quasars. These observations reveal that the quasars host supermassive black holes with masses exceeding $10^9 M_\odot$ in many cases (e.g., Jiang et al. 2007; Kurk et al. 2007; De Rosa et al. 2011, 2014; Venemans et al. 2015; Wu et al. 2015). Likewise, observations in the (sub)millimeter regime have the potential to trace the rest-frame far-infrared (FIR) emission in the quasar host, as well as key diagnostic lines of their interstellar medium (ISM, see, e.g., Carilli & Walter 2013).

Initial studies of the galaxies that host luminous quasars at $z \sim 6$ unveiled that roughly 30% of quasar hosts were bright at mm wavelengths ($S_{250\text{ GHz}} \gtrsim 1$ mJy), implying FIR luminosities $L_{\text{FIR}} \gtrsim 3 \times 10^{12} L_\odot$ and star-formation rates (SFRs) possibly exceeding $1000 M_\odot \text{ yr}^{-1}$ (e.g., Bertoldi et al. 2003a; Wang et al. 2007, 2008, 2016). Follow-up studies of these FIR-bright quasar hosts targeting the redshifted CO emission line revealed that these galaxies have large reservoirs of cold molecular gas (e.g., Bertoldi et al. 2003b; Walter et al. 2003; Carilli et al. 2007; Wang et al. 2010, 2011a, 2011b, 2016). These early studies of the host galaxies of $z \sim 6$ quasars naturally concentrated on FIR-bright quasars, and the results from these studies may introduce a biased view on the

characteristics of the typical galaxy hosting a $z \sim 6$ quasar. This is supported by studies of lower-luminosity $z \sim 6$ quasars, powered by black holes with a mass of “only” $10^8 M_\odot$, that reveal hosts with significantly fainter FIR luminosities of $L_{\text{FIR}} \approx 10^{11} L_\odot$ and SFRs of $\text{SFR} \ll 100 M_\odot \text{ yr}^{-1}$ (Willott et al. 2013, 2015).

To extend the study of quasar host galaxies to $z \sim 7$ we initiated a program targeting all quasars discovered at $z > 6.5$ in [C II] line emission and the underlying continuum, independent of their FIR brightness, with the aim of sampling the range of properties of quasar host galaxies and investigating the star formation–supermassive black hole growth relation at $z \sim 7$. The first quasar targeted in this project, J1120+0641 at $z = 7.1$, already displayed somewhat different characteristics in its FIR properties (a fainter FIR luminosity of $L_{\text{FIR}} = (6\text{--}18) \times 10^{11} L_\odot$ and a more compact, ~ 1 kpc host galaxy; Venemans et al. 2012, 2017) from the well-studied $z \sim 6$ quasar hosts. Subsequent imaging of the FIR continuum and the [C II] 158 μm emission line of additional $z > 6.5$ quasars showed a range of properties, with FIR luminosities from $L_{\text{FIR}} \lesssim 10^{12} L_\odot$ to $L_{\text{FIR}} \sim 10^{13} L_\odot$ (Bañados et al. 2015; Venemans et al. 2016, 2017; Decarli et al. 2017; Mazzucchelli et al. 2017).

So far, our sample of $z > 6.5$ quasar hosts has primarily been observed at 1 mm, targeting the [C II] line and the underlying FIR continuum at 160 μm in the rest-frame. To further study the characteristics of the ISM in $z > 6.5$ quasar host galaxies, it is imperative to detect the FIR continuum of these galaxies at different frequencies and to observe additional molecular or atomic lines. In this paper, we present ALMA

Cycle 2 observations of the CO(6–5), CO(7–6), and [C I](2–1) 369 μm (hereafter [C I]) emission lines and the underlying dust continuum in three quasar host galaxies at $6.6 < z < 6.9$. These quasar host galaxies are VIKING J030516.92–315056.0 (hereafter J0305–3150) at $z = 6.6$, VIKING J010953.13–304726.3 (hereafter J0109–3040) at $z = 6.8$, and VIKING J234833.34–305410.0 (hereafter J2348–3054) at $z = 6.9$, discovered in Venemans et al. (2013). At the time of discovery, these three sources were the only quasars known at $z > 6.5$ besides J1120+0641 at $z = 7.1$ (Mortlock et al. 2011). The absolute magnitudes at 1450 \AA in the rest-frame of these VIKING quasars are between –26.0 and –25.5, which is 1.4–1.9 mag fainter than PSO J036.5078+03.0498 at $z = 6.54$, the most luminous $z > 6.5$ quasar currently known (Venemans et al. 2015) and >0.6 mag brighter than the faint quasar J1205–0000 at $z \approx 6.7$ discovered with the Subaru Hyper Suprime-Cam (Matsuoka et al. 2016). The VIKING quasars are powered by black holes with masses of $\sim(1\text{--}2) \times 10^9 M_\odot$ (Venemans et al. 2013; De Rosa et al. 2014). These black hole masses are comparable to those of other $z > 6.5$ quasars (e.g., Mortlock et al. 2011; De Rosa et al. 2014; Venemans et al. 2015, Mazzucchelli et al. 2017). The three VIKING quasars were previously observed with ALMA in Cycle 1 at ~ 1 mm, targeting the redshifted [C II] emission line (presented in Venemans et al. 2016). All three quasar host galaxies were detected with [C II] luminosities ranging between $(1.9\text{--}3.9) \times 10^9 L_\odot$ and continuum luminosities at a rest-frame wavelength of 158 μm of νL_ν (158 μm) = $(0.8\text{--}4.3) \times 10^{45} \text{ erg s}^{-1}$ (see Table 1). The additional CO and [C I] observations presented here, as well as the measurement of the underlying dust continuum emission at observed wavelengths around 3 mm (rest-frame wavelengths around 400 μm), allow us, for the first time, to constrain the physical properties of quasar host galaxies at $z \sim 7$ in more detail.

The paper is organized as follows. In Section 2 a description of the ALMA Cycle 2 observations is given. In Section 3 we present our results; in Sections 3.1–3.3 we provide the derived properties for each of the three sources. In Section 4 we discuss our results; in Section 4.1 we compare the dust continuum measurements made at 3 mm (observed) with those at 1 mm, to constrain the shape of the dust spectral energy distribution, and in Sections 4.2 and 4.3 we estimate the molecular gas and atomic carbon mass from the detected emission lines; in Section 4.4 we provide constraints on the properties of the ISM, followed by a summary in Section 5.

Throughout this paper, we adopt a concordance cosmology with parameters: $H_0 = 70 \text{ km s}^{-1} \text{ Mpc}^{-1}$, $\Omega_M = 0.3$, and $\Omega_\Lambda = 0.7$.

2. ALMA Observations

The three quasar host galaxies were observed in ALMA band 3 with 39–40 antennas in a compact configuration (baselines between 15 and 349 m) between 2014 December 29 and 2015 January 6. A summary of the observations is given in Table 1. On 2014 December 29 J0109–3047 was observed for 47 minutes (24 minutes on-source), on 2014 December 30 observations of J2348–3054 were carried out for 60 minutes, of which 34 minutes were on-source, and on 2015 January 6 the host galaxy of J0305–3150 was observed for 31 minutes (16 minutes on-source). Our setup consisted of two pairs of two spectral windows, with each spectral window covering a

frequency range of 1.875 GHz at a resolution of 3.9 MHz (11–13 km s^{-1}). The two pairs of spectral windows are placed in sidebands that are separated by ~ 12 GHz. By fortuitous coincidence the frequency range that can be covered in this setup allows us to image two CO lines simultaneously for sources at $z \gtrsim 6.5$.

For all three quasar hosts the setup was tuned to include the CO(6–5) line in one of the four sidebands and the CO(7–6) and [C I] lines in another sideband, using the redshift from the previous [C II] observations. The two remaining spectral windows were placed between the CO(6–5) and CO(7–6) lines and utilized to increase the signal-to-noise (S/N) of the continuum measurement. The beam size of $>2''(>12 \text{ kpc})$ ensured that the emission was likely unresolved by the ALMA observations, as the maximum extent of the [C II] emission in these sources is $<0''.6$ (Venemans et al. 2016). For bandpass calibration, the sources J2258–2758, J2357–5311, and J0519–4546 were observed, respectively. The amplitude and flux calibration were performed through observations of the source J0334–401 and Mars, and the calibrators J2359–3133, J0120–2701, and J0334–4008, respectively, were observed every ~ 7 minutes for phase calibration. The raw data were reduced following standard reduction steps in the Common Astronomy Software Applications package (McMullin et al. 2007). The reduced cubes were cleaned with a weighting factor of robust = 2 (equivalent to natural weighting) to obtain the lowest noise maps. The rms noise per 100 MHz bins averaged between 0.10 and 0.24 mJy (Table 1).

3. CO and [C I] Spectra

In Figure 1 we show the CO and [C I] spectra of the quasar hosts extracted at the position of the center of the [C II] emission. We fitted a Gaussian function to the lines, fixing the redshift and the width of the lines to those from the significantly higher S/N [C II] line (Venemans et al. 2016). In Figure 2 we averaged the data at the redshift given by the [C II] line over the width of the [C II] line. Channels not belonging to emission lines were averaged to create continuum maps. Below, we will describe the results for each of the sources individually.

3.1. J0305–3150 ($z_{[\text{C II}]} = 6.6145$)

The host galaxy of quasar J0305–3150 shows the brightest [C II] line of the three VIKING quasars presented in Venemans et al. (2016). The [C II] line was detected at a redshift of $z_{[\text{C II}]} = 6.6145 \pm 0.0001$ with a strength of $F_{[\text{C II}]} = 3.44 \pm 0.15 \text{ Jy km s}^{-1}$ and a width of $\text{FWHM} = 255 \pm 12 \text{ km s}^{-1}$. Fitting a Gaussian with a FWHM of 255 km s^{-1} centered on the (redshifted) frequency of the CO(6–5) emission line ($\nu_{\text{CO}(6\text{--}5),\text{obs}} = \nu_{\text{CO}(6\text{--}5),\text{rest}} / (1 + z_{[\text{C II}]})$) to the spectrum (Figure 1) resulted in a $\sim 8\sigma$ detection (Figure 2) of the CO(6–5) line, with a strength of $0.65 \pm 0.07 \text{ Jy km s}^{-1}$ and a luminosity of $L_{\text{CO}(6\text{--}5)} = (2.6 \pm 0.3) \times 10^8 L_\odot$. Allowing the width and center of the Gaussian to vary gives very similar parameters: $z_{\text{CO}(6\text{--}5)} = 6.6139 \pm 0.0005$, $\text{FWHM}_{\text{CO}(6\text{--}5)} = 314 \pm 48 \text{ km s}^{-1}$, and $F_{\text{CO}(6\text{--}5)} = 0.74 \pm 0.10 \text{ Jy km s}^{-1}$.

The CO(7–6) emission line was detected at $\sim 6\sigma$ with $z_{\text{CO}(7\text{--}6)} = 6.6155 \pm 0.0004$, $\text{FWHM}_{\text{CO}(7\text{--}6)} = 225 \pm 38 \text{ km s}^{-1}$, and $F_{\text{CO}(7\text{--}6)} = 0.68 \pm 0.10 \text{ Jy km s}^{-1}$. Forcing the

Table 1
Properties of the Observed Quasar Host Galaxies, Description of the ALMA Cycle 2 Observations, and the Derived Characteristics of the Hosts

	J0305–3150	J0109–3047	J2348–3054
R.A. (J2000)	03 ^h 05 ^m 16 ^s .91	01 ^h 09 ^m 53 ^s .13	23 ^h 48 ^m 33 ^s .35
Decl. (J2000)	−31°50'55"94	−30°47'26"32	−30°54'10"30
$z_{[\text{C II}]}$	6.6145 ± 0.0001	6.7909 ± 0.0004	6.9018 ± 0.0007
$L_{[\text{C II}]} (L_\odot)$	$(3.9 \pm 0.2) \times 10^9$	$(2.4 \pm 0.2) \times 10^9$	$(1.9 \pm 0.3) \times 10^9$
FWHM _[\text{C II}] (km s ^{−1})	255 ± 12	340 ± 34	405 ± 69
$L_{\text{FIR}} (L_\odot)$ ^a	$(7.3^{+0.2}_{-3.3}) \times 10^{12}$	$(1.3^{+0.2}_{-0.7}) \times 10^{12}$	$(4.5^{+0.4}_{-2.3}) \times 10^{12}$
$M_d (M_\odot)$ ^a	$(4.5\text{--}24) \times 10^8$	$(0.7\text{--}4.9) \times 10^8$	$(2.7\text{--}15) \times 10^8$
ν_{obs} (GHz)	90.6–94.4, 102.6–106.5	88.4–92.2, 100.4–104.2	87.0–90.8, 99.0–102.9
$t_{\text{exp, on-source}}$ (minutes)	16	24	34
# of antennas	39	40	39
RMS noise (per 100 MHz)	242 μJy	121 μJy	102 μJy
beam size	5''.3 × 2''.2	4''.2 × 2''.5	3''.8 × 2''.3
CO(6–5) flux (Jy km s ^{−1})	0.65 ± 0.07	0.11 ± 0.05	0.28 ± 0.05
$L_{\text{CO}(6-5)} (L_\odot)$	$(2.6 \pm 0.3) \times 10^8$	$(4.4 \pm 1.9) \times 10^7$	$(1.2 \pm 0.2) \times 10^8$
$L'_{\text{CO}(6-5)} (\text{K km s}^{-1} \text{ pc}^2)$	$(2.6 \pm 0.3) \times 10^{10}$	$(4.5 \pm 2.0) \times 10^9$	$(1.2 \pm 0.2) \times 10^{10}$
CO(7–6) flux (Jy km s ^{−1})	0.69 ± 0.09	0.24 ± 0.04	0.26 ± 0.06
$L_{\text{CO}(7-6)} (L_\odot)$	$(3.2 \pm 0.4) \times 10^8$	$(1.2 \pm 0.2) \times 10^8$	$(1.3 \pm 0.3) \times 10^8$
$L'_{\text{CO}(7-6)} (\text{K km s}^{-1} \text{ pc}^2)$	$(2.0 \pm 0.3) \times 10^{10}$	$(7.5 \pm 1.3) \times 10^9$	$(8.1 \pm 1.7) \times 10^9$
[C I](2–1) flux (Jy km s ^{−1})	<0.35	<0.15	0.16 ± 0.06
$L_{[\text{C I}](2-1)} (L_\odot)$	<1.6 × 10 ⁸	<7.4 × 10 ⁷	$(8.0 \pm 2.8) \times 10^7$
$L'_{[\text{C I}](2-1)} (\text{K km s}^{-1} \text{ pc}^2)$	<9.6 × 10 ⁹	<4.4 × 10 ⁹	$(4.7 \pm 1.7) \times 10^9$
$S_{3 \text{ mm}}$ (μJy)	233 ± 30	<46	118 ± 13
$L'_{\text{CO}(1-0)}$ ^b (K km s ^{−1} pc ²)	$(3.4 \pm 0.3) \times 10^{10}$	$(1.3 \pm 0.2) \times 10^{10}$	$(1.4 \pm 0.2) \times 10^{10}$
$L_{[\text{C II}]} / L_{\text{CO}(1-0)}$ ^b	2530 ± 130	4170 ± 350	2860 ± 450
$M_{\text{H}_2,\text{CO}}$ (M_\odot) ^c	$(2.7 \pm 0.2) \times 10^{10}$	$(1.0 \pm 0.2) \times 10^{10}$	$(1.2 \pm 0.2) \times 10^{10}$
$M_{\text{H}_2,\text{dust}}$ (M_\odot) ^d	$(2.4\text{--}18) \times 10^{10}$	$(0.4\text{--}3.7) \times 10^{10}$	$(1.4\text{--}11) \times 10^{10}$
$M_{\text{C I}}$ (M_\odot) ^e	<2.1 × 10 ⁷	<9.6 × 10 ⁶	$(1.0 \pm 0.4) \times 10^7$

Notes.

^a L_{FIR} and M_d are derived from the continuum detection at 1 mm, taken from Venemans et al. (2016).

^b A CO excitation ladder similar to that of the $z = 6.4$ quasar J1148+5251 is assumed (see Section 4.2).

^c Molecular gas mass derived from the CO(1–0) luminosity, assuming a luminosity-to-gas mass conversion factor of $\alpha = 0.8 M_\odot (\text{K km s}^{-1} \text{ pc}^2)^{-1}$.

^d Molecular gas mass derived from the dust mass, assuming a gas-to-dust mass ratio of 70–100 and a molecular gas mass fraction of 0.75 (see Section 4.2).

^e Assuming an excitation temperature of $T_{\text{ex}} = 30$ K (see Section 4.3).

line to have the same width and redshift as the [C II] line results in a similar line strength as the values above, 0.69 ± 0.09 Jy km s^{−1}, and a CO(7–6) luminosity of $L_{\text{CO}(7-6)} = (3.2 \pm 0.4) \times 10^8 L_\odot$. The width, redshift, and spatial location of the CO(6–5) and CO(7–6) emission are, within the uncertainties, consistent with those of the [C II] line. This indicates that gas components traced by the [C II] and CO emission have, on average, similar kinematics.

The measured CO fluxes of $F_{\text{CO}(6-5)} = 0.65$ Jy km s^{−1} and $F_{\text{CO}(7-6)} = 0.69$ Jy km s^{−1} make the host of J0305–3150 roughly as bright as the archetypical, luminous SDSS quasar J1148+5251 (which has $F_{\text{CO}(6-5)} = 0.67$ Jy km s^{−1} and $F_{\text{CO}(7-6)} = 0.63$ Jy km s^{−1}; Bertoldi et al. 2003b; Walter et al. 2003; Riechers et al. 2009).

The [C I] emission line has not been significantly detected in both the spectrum and the line map (Figures 1 and 2). At the position and redshift of the [C II] emission, we measure a 3σ upper limit to the line flux of $F_{[\text{C I}]} < 0.35$ Jy km s^{−1} ($L_{[\text{C I}]} < 1.6 \times 10^8 L_\odot$).

Averaging the frequency channels not covered by emission lines resulted in a significant, 8σ detection of the continuum at an observed frequency of 98.4 GHz (rest-frame frequency of

749 GHz, rest-frame wavelength of $\sim 400 \mu\text{m}$) of $S_{98.4 \text{ GHz}} = 233 \pm 30$ μJy. We will discuss the implications of this detection further in Section 4.1.

3.2. J0109–3047 ($z_{[\text{C II}]} = 6.7909$)

The host galaxy of quasar J0109–3047 was detected in [C II] with $z_{[\text{C II}]} = 6.7909 \pm 0.0004$, $F_{[\text{C II}]} = 2.04 \pm 0.20$ Jy km s^{−1}, and a width of FWHM = 340 ± 36 (Venemans et al. 2016). The continuum of the host was the faintest of the three quasars considered here, with $S_{1 \text{ mm}} = 0.56 \pm 0.11$ mJy at 158 μm in the rest-frame.

The CO(6–5) line is only marginally detected in this quasar host, with an S/N ≈ 2.3 (Figures 1 and 2). From a fit to the spectrum, we derive a line flux of $F_{\text{CO}(6-5)} = 0.11 \pm 0.05$ Jy km s^{−1} and a luminosity of $L_{\text{CO}(6-5)} = (4.4 \pm 1.9) \times 10^7 L_\odot$. In contrast, the CO(7–6) line was detected with an S/N ≈ 6 at the same spatial position as the [C II] line in the line map (Figure 2). Fitting a Gaussian to the spectrum while fixing the width and redshift to that of the [C II] line gives a line strength of $F_{\text{CO}(7-6)} = 0.24 \pm 0.04$ Jy km s^{−1} ($L_{\text{CO}(7-6)} = (1.2 \pm 0.2) \times 10^8 L_\odot$). We do not detect the [C I] line, and place 3σ limits on the line flux of $F_{[\text{C I}]} < 0.15$ Jy km s^{−1} ($L_{[\text{C I}]} < 7.4 \times 10^7 L_\odot$).

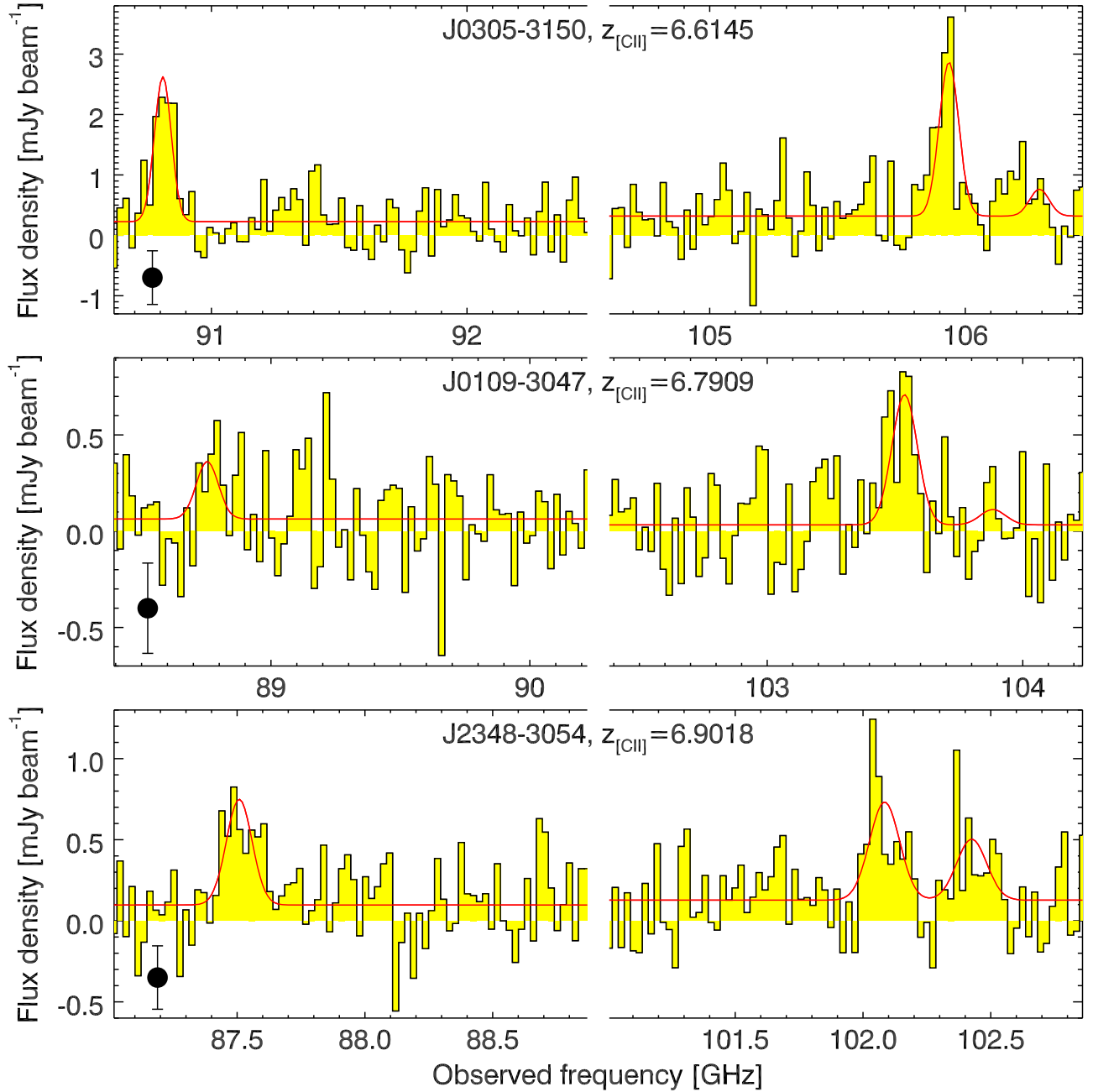


Figure 1. ALMA 3 mm spectra containing the CO and [C I] emission lines of the three $6.6 < z < 6.9$ quasar host galaxies, extracted at the position of the [C II] emission (that is coincident with the quasar position). The channels were binned by a factor of 6 to a width of 23.4 MHz ($\sim 80 \text{ km s}^{-1}$). The typical uncertainty per bin is shown in the lower left corner. The red solid line shows a fit to the CO(6–5), CO(7–6), and [C I] lines, with the redshift and line width fixed to those of the [C II] emission line (see Table 1).

The host galaxy of J0109–3047 was not detected in the 3 mm continuum image (Figure 2). At the position of the quasar host galaxy we measure a continuum flux density of $S_{9.6 \text{ GHz}} = 22 \pm 15 \mu\text{Jy}$ (corresponding to a rest-frame frequency of 750 GHz). The 3σ upper limit for the continuum flux density is $46 \mu\text{Jy}$.

3.3. J2348–3054 ($z_{[\text{C II}]} = 6.9018$)

J2348–3054 is the highest-redshift quasar in our sample, with $z_{[\text{C II}]} = 6.9018 \pm 0.0007$. It has the faintest [C II] line of our three observed quasars, with $F_{[\text{C II}]} = 1.57 \pm 0.26 \text{ Jy km s}^{-1}$ and $\text{FWHM}_{[\text{C II}]} = 405 \pm 69 \text{ km s}^{-1}$ (Venemans et al. 2016).

Both the CO(6–5) and CO(7–6) lines are detected at S/N ~ 5 in the ALMA band 3 data (Figures 1 and 2). The line fluxes measured from the spectrum, using the [C II] redshift and line width, are $F_{\text{CO}(6-5)} = 0.28 \pm 0.05 \text{ Jy km s}^{-1}$ and $F_{\text{CO}(7-6)} = 0.26 \pm 0.06 \text{ Jy km s}^{-1}$. This corresponds to line luminosities of $L_{\text{CO}(6-5)} = (1.2 \pm 0.2) \times 10^8 L_\odot$ and $L_{\text{CO}(7-6)} = (1.3 \pm 0.3) \times 10^8 L_\odot$, which is very similar to the CO(7–6) luminosity of J0109–3047.

Intriguingly, the [C I] line in J2348–3054 was also detected, albeit with a low significance ($S/N \sim 3$). Both in frequency (Figure 1) and spatially (Figure 2), the [C I] emission coincides with the expectations from the [C II] emission line. We derive a line flux of $F_{[\text{C I}]} = 0.16 \pm 0.06 \text{ Jy km s}^{-1}$ and a luminosity of

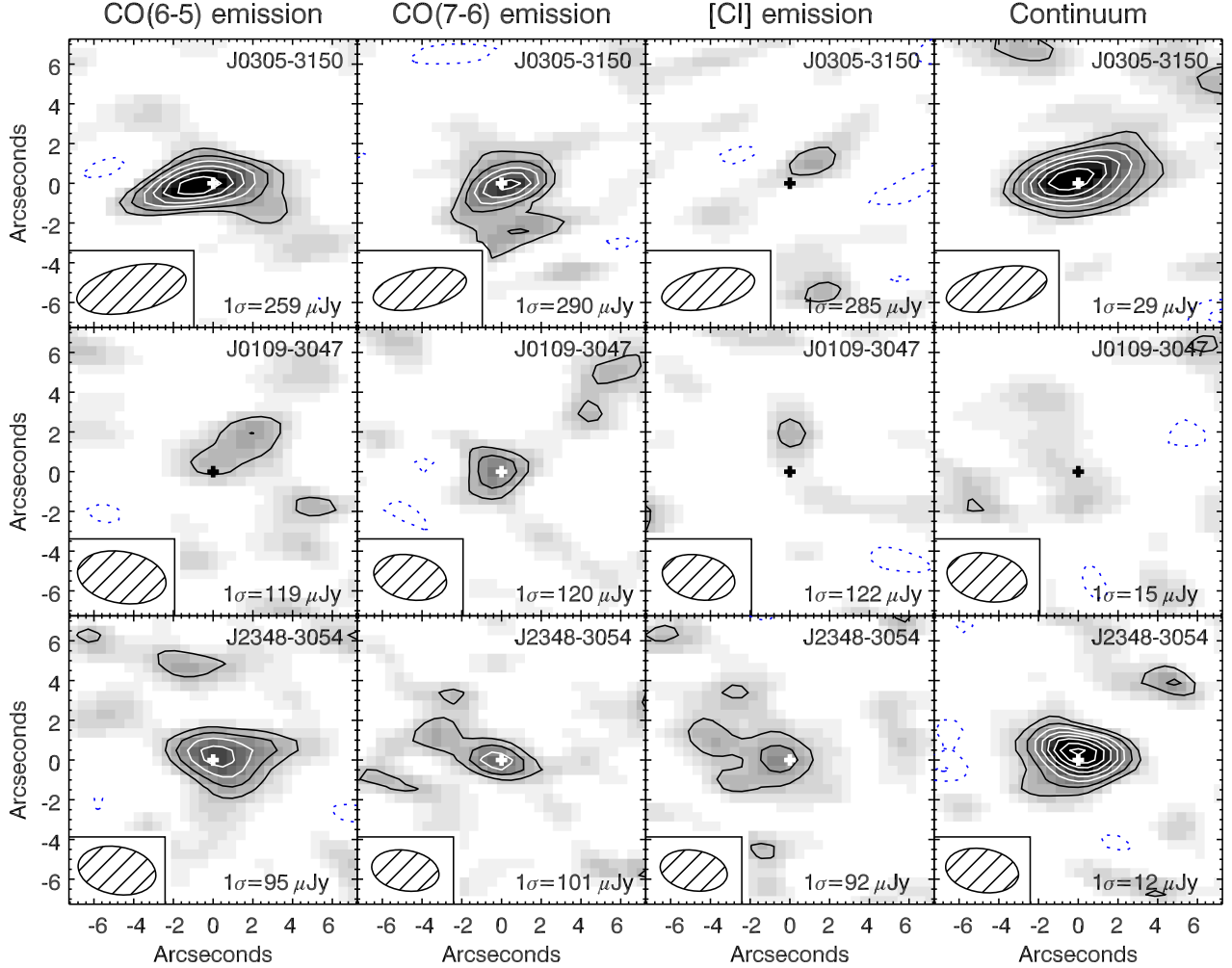


Figure 2. Maps of the line and continuum emission from the three quasar host galaxies. From left to right, the CO(6–5), CO(7–6), [C I], and underlying continuum emission are shown. To create the line emission maps, the data cubes were first continuum-subtracted and subsequently averaged over the FWHM of the [C II] line (405 km s^{-1} , 340 km s^{-1} , and 255 km s^{-1} for J2348–3054, J0109–3047, and J0305–3150, respectively, see Table 1). The beam is shown in the bottom left of each map and in the bottom right the 1σ rms noise is printed. The blue, dashed contours are -3σ and -2σ , the black, solid contours are $+2\sigma$ and $+3\sigma$, and the white solid contours are $[4, 5, 6, 7, 8, 9] \times \sigma$. The small white and black crosses indicate the position of the [C II] emission of quasar host galaxies.

$L_{[\text{C I}]} = (8.0 \pm 2.8) \times 10^7 L_\odot$ from the spectrum. We will discuss the implications of the detection of this line in Section 4.3.

The continuum of J2348–3054 was also detected (Figure 2) with $S_{94.9 \text{ GHz}} = 118 \pm 13 \mu\text{Jy}$ ($\text{S/N} \sim 9$).

4. Discussion

4.1. Constraints on the Dust Emission

Analysis of the far-infrared emission in luminous, high-redshift ($z \gtrsim 2$) quasars revealed that the dust in these objects has typical temperatures between 40 and 60 K, with a mean of $T_d = 47 \pm 3$ K (e.g., Priddey & McMahon 2001; Beelen et al. 2006; Leipski et al. 2014). A dust temperature of $T_d = 47$ K has subsequently often been assumed for studies of the cold dust emission of $z \gtrsim 6$ quasar hosts (e.g., Wang et al. 2013; Willott et al. 2013, 2015; Bañados et al. 2015; Venemans et al. 2016). In this section we combine the continuum measurements from our ALMA 1 mm data (presented in Venemans et al. 2016) with the continuum detections in the 3 mm data presented here, to test whether the dust temperature is consistent with the canonical value. The addition of a

continuum point at 3 mm significantly increases the baseline over which we can constrain the dust SED. However, both our continuum points are on the Rayleigh–Jeans tail of the dust emission and we cannot tightly constrain the dust temperature at these relatively long wavelengths. Furthermore, we need to make assumptions about the properties of the dust. Following the literature, we here assume that the dust emission can be described by a modified blackbody with a dust temperature T_d and a power-law emissivity index β (e.g., Priddey & McMahon 2001; Venemans et al. 2016). With only two continuum detections (at ~ 1 mm and ~ 3 mm), we cannot constrain T_d and β at the same time. In the following discussion, we will assume two different values of β from the literature: $\beta = 1.6$ (Beelen et al. 2006) and $\beta = 1.95$ (Priddey & McMahon 2001).

As discussed in Venemans et al. (2016), it is important to take the effects of the CMB into account, which has a temperature of $T_{\text{CMB}} \approx 21$ K at $z = 6.8$. The CMB provides both an additional source of heating and a background that reduces the detectability of the emission from the quasar hosts; see da Cunha et al. (2013) for an extensive discussion on these effects. While the heating by the CMB is negligible for our

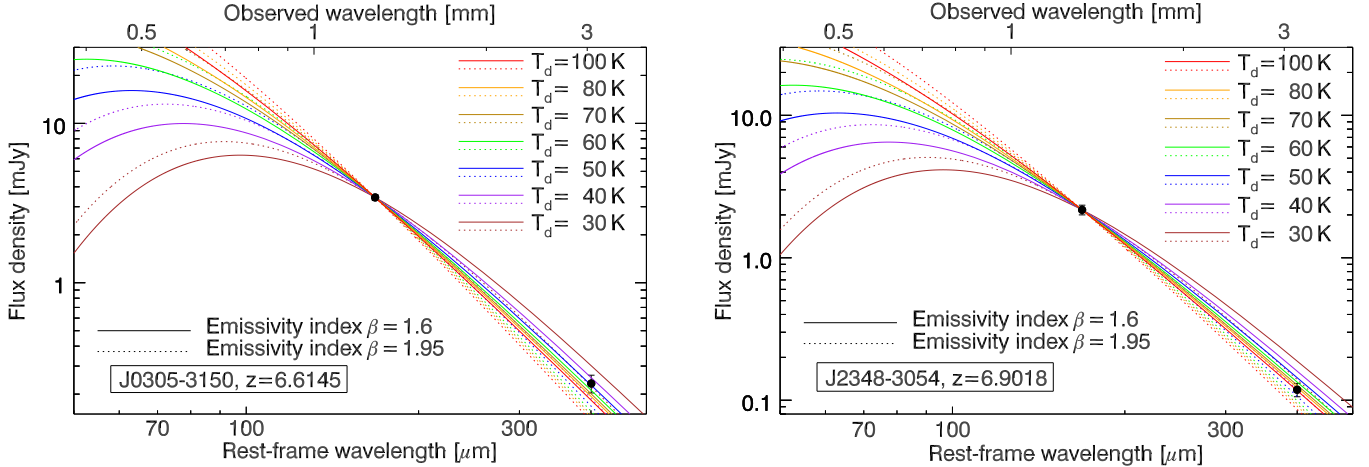


Figure 3. Measured flux densities at observed wavelengths around 1 mm and 3 mm of the far-infrared dust continuum in J0305–3150 (left) and J2348–3054 (right). Overplotted are modified blackbody curves with different temperatures for two dust emissivity indices ($\beta = 1.6$ and $\beta = 1.95$) fixed to the data point at 1.3 mm. The solid lines show the observed dust SED assuming $\beta = 1.6$, while the dashed line assumes an emissivity index of $\beta = 1.95$. With β fixed to $\beta = 1.6$ we derive best-fitting temperatures of $T_d = 47^{+21}_{-10}$ K for J0305–3150 and $T_d = 94^{+174}_{-35}$ K for J2348–3054. For $\beta = 1.95$, we find $T_d = 28^{+7}_{-5}$ K and $T_d = 40^{+13}_{-8}$ K for J0305–3150 and J2348–3054, respectively. The upper limit on the 3 mm continuum strength that we derive for J0109–3047 results in a lower limit of $T_d > 27$ K in this quasar host (Section 4.1). To better constrain the temperature, continuum detections at smaller wavelengths are required.

sources, if the dust temperature is $T_d \gtrsim 30$ K, the CMB can significantly reduce the flux density we measure from a source at high redshift, especially the low frequencies:

$$S_\nu^{\text{obs}} / S_\nu^{\text{intrinsic}} = 1 - B_\nu[T_{\text{CMB}}(z)] / B_\nu[T_d], \quad (1)$$

with B_ν being the Planck function at rest-frame frequency ν (da Cunha et al. 2013), i.e., with a dust temperature of $T_d = 30$ K and a redshift of $z = 6.6$, we are only measuring 75% and 50% of the intrinsic flux density at rest-frame wavelengths of 158 μm and 400 μm , respectively.

To compare the continuum flux densities at 1 mm with those measured at 3 mm, we first averaged the line-free sidebands at 1 mm and subsequently convolved the resulting image to the same resolution as the 3 mm data. For J0305–3150 we measure $S_{234.6 \text{ GHz}} = 3.43 \pm 0.37$ mJy. The observed flux ratio in the two ALMA bands is thus $S_{1 \text{ mm}} / S_{3 \text{ mm}} = 14.7$. This is very similar to the ratio of $S_{1 \text{ mm}} / S_{3 \text{ mm}} \sim 14$ measured in the well-studied quasar host J1148+5251 at $z = 6.42$ (Riechers et al. 2009; Gallerani et al. 2014). For J2348–3054 we measure $S_{225.4 \text{ GHz}} = 2.17 \pm 0.17$ mJy and $S_{1 \text{ mm}} / S_{3 \text{ mm}} = 18.3$.

In Figure 3 we show the continuum detections of the host galaxies of bf J0305–3150 and J2348–3054. We fitted a modified blackbody to the data points, taking into account the effects of the CMB described above, with fixed redshifts of $z = 6.6145$ and $z = 6.9018$, respectively, and two different dust emissivity indices of $\beta = 1.6$ and $\beta = 1.95$. We added an uncertainty of 10% in quadrature to account for the absolute flux calibration uncertainty. We derive a dust temperature of $T_d = 47^{+21}_{-10}$ K ($T_d = 28^{+7}_{-5}$ K) assuming a $\beta = 1.6$ ($\beta = 1.95$) for J0305–3150 and $T_d = 94^{+174}_{-35}$ K ($T_d = 40^{+13}_{-8}$ K) for J2348–3054. Within the large uncertainties, these values are consistent with the canonical values of $T_d = 41$ –47 K. If instead we fix the dust temperature to $T_d = 47$ K, we derive values for the dust emissivity index of $\beta = 1.60^{+0.16}_{-0.15}$ for J0305–3150 and $\beta = 1.86 \pm 0.15$ for J2348–3054. As is demonstrated in Figure 3, our observed continuum flux densities at 1 mm and 3 mm do not pose tight constraints on the dust temperature and emissivity index. To better constrain the dust temperature, we need to measure the dust continuum at

rest-frame wavelengths $< 100 \mu\text{m}$ in these quasar hosts. This is feasible with, for example, ALMA band 8 and 9 observations.

The 3 mm continuum was not detected in the host galaxy of quasar J0109–3047, and we therefore could not constrain the dust temperature in this source. By taking the 3σ upper limit of $S_{3 \text{ mm}} = 0.046$ mJy, we derived a lower limit on the dust temperature of $T_d > 27$ K. For a dust temperature of $T_d = 47$ K and $\beta = 1.6$, we expect, based on the continuum detection at ~ 1 mm, a 3 mm continuum flux density of $S_{96.3 \text{ GHz}} \approx 33 \mu\text{Jy}$, which is consistent with our observed limits.

In the remainder of this paper, we will use the FIR luminosities derived from the continuum detection at 1 mm by Venemans et al. (2016). These values are listed in Table 1. The FIR luminosity is obtained by assuming $T_d = 47$ K and $\beta = 1.6$, while the error bar includes both the measurement error and the uncertain shape of FIR continuum. The latter is determined by scaling model templates of local star-forming galaxies to the continuum detection; see Venemans et al. (2016) for details.

4.2. Molecular Gas Mass Derived from CO

The mass of the molecular (mostly H₂) gas can be estimated using the equation $M_{\text{gas}} = \alpha L'_{\text{CO}(1-0)}$, with M_{gas} being the molecular gas mass, α the CO luminosity-to-gas mass conversion factor, and $L'_{\text{CO}(1-0)}$ the CO(1–0) luminosity in units of $\text{K km s}^{-1} \text{ pc}^2$. The luminosity of an emission line can be derived by

$$\begin{aligned} L'_{\text{line}} &= L_{\text{line}} / (3 \times 10^{-11} \nu_{\text{rest}}^3) = \\ &= 3.25 \times 10^7 F_{\text{line}} D_L^2 (1+z)^{-3} \nu_{\text{obs}}^{-2}, \end{aligned} \quad (2)$$

with ν_{rest} and ν_{obs} being the rest-frame and observed frequency of the emission line in GHz, D_L the luminosity distance in Mpc, and F_{line} the line flux in Jy km s^{-1} (e.g., Carilli & Walter 2013). Following the literature, we further assume a value of $\alpha = 0.8 M_\odot (\text{K km s}^{-1} \text{ pc}^2)^{-1}$, derived for local ultra-luminous infrared galaxies (ULIRGs; e.g., Downes & Solomon 1998). This value is also used to compute molecular gas masses in $z \sim 6$ quasar host galaxies (e.g., Wang et al. 2010).

Since we only measured the CO(6–5) and/or CO(7–6) line flux in our sources, we have to assume a CO spectral line energy distribution (CO SLED) to estimate the CO(1–0) line strength. The CO emission of distant quasars peaks around that of CO(6–5) and CO(7–6) (e.g., Riechers et al. 2009; Carilli & Walter 2013). To estimate CO(1–0) luminosity in our sources, here we apply the same model that fits the strength of the CO lines of the quasar host galaxy J1148+5251 at $z = 6.42$ (Riechers et al. 2009; Stefan et al. 2015). In J1148+5251, several low- J and high- J CO lines have been detected, including the CO(2–1), CO(3–2), CO(6–5), and CO(7–6) lines (Bertoldi et al. 2003b; Walter et al. 2003; Riechers et al. 2009; Stefan et al. 2015). The large velocity gradient (LVG) model by Riechers et al. (2009) that fits the observed CO line fluxes in J1148+5251 results in observed CO(6–5) and CO(7–6) line fluxes that are of roughly equal strength, $F_{\text{CO}(7-6)}/F_{\text{CO}(6-5)} = 1.03$, and line flux ratios of $F_{\text{CO}(6-5)}/F_{\text{CO}(1-0)} = 28$ and $F_{\text{CO}(7-6)}/F_{\text{CO}(1-0)} = 29$. Following Equation (2), the CO luminosity ratios of the LVG model are $L'_{\text{CO}(6-5)}/L'_{\text{CO}(1-0)} \approx 0.78$ and $L'_{\text{CO}(7-6)}/L'_{\text{CO}(1-0)} \approx 0.60$. Note that in the two cases where we detect both CO(6–5) and CO(7–6) lines, the ratio is indeed close to 1 (Table 1): $F_{\text{CO}(7-6)}/F_{\text{CO}(6-5)} \approx 1.06$ and $F_{\text{CO}(7-6)}/F_{\text{CO}(6-5)} \approx 0.93$ for J0305–3150 and J2348–3054, respectively.

Using Equation (2), we derive CO(6–5) and CO(7–6) luminosities in our quasar hosts of $L'_{\text{CO}(6-5)} = (0.45-2.6) \times 10^{10} \text{ K km s}^{-1} \text{ pc}^2$ and $L'_{\text{CO}(7-6)} = (0.75-2.0) \times 10^{10} \text{ K km s}^{-1} \text{ pc}^2$ (see Table 1). Assuming that the CO excitation ladder in the VIKING quasar hosts can be described with the one derived for J1148+5251, we can obtain $L'_{\text{CO}(1-0)}$ luminosities by applying the $L'_{\text{CO}(6-5)}/L'_{\text{CO}(1-0)}$ and $L'_{\text{CO}(7-6)}/L'_{\text{CO}(1-0)}$ luminosity ratios given by the LVG model. For J0305–3150 and J2348–3054, where we detect both CO(6–5) and CO(7–6) lines at $\text{S/N} > 3$, we take the weighted mean of the two estimated CO(1–0) luminosities. For J0109–3047 we only consider the CO(7–6) line, as the CO(6–5) line has a low significance (Figures 1 and 2). The CO(1–0) luminosities we derive for the quasar hosts are $L'_{\text{CO}(1-0),\text{J0305}-3150} = (3.4 \pm 0.4) \times 10^{10}$, $L'_{\text{CO}(1-0),\text{J0109}-3047} = (1.3 \pm 0.2) \times 10^{10}$, and $L'_{\text{CO}(1-0),\text{J2348}-3054} = (1.4 \pm 0.2) \times 10^{10} \text{ K km s}^{-1} \text{ pc}^2$.

The [C II]/CO(1–0) luminosity ratios derived for the three quasar hosts range from 2500 to 4200. These values are within a factor of 2 of the ratio of $L_{[\text{C II}]}/L_{\text{CO}(1-0)} \approx 4100$ measured in local starburst galaxies and star-forming regions in the Milky Way (e.g., Stacey et al. 1991) and in dusty star-forming galaxies at $z > 2$ (e.g., Gullberg et al. 2015). In Figure 4 we plot the FIR luminosity against the CO(1–0) luminosity $L'_{\text{CO}(1-0)}$ of our quasar hosts. The CO and FIR luminosities of J0305–3150 and J2348–3054 are very similar to those in $z \sim 6$ quasar host galaxies (e.g., Wang et al. 2010, 2011a, 2011b). The $z > 6.6$ host galaxies discussed here have CO(1–0) over FIR luminosity ratios consistent with those of starburst galaxies at $z = 0-3.5$ (e.g., Daddi et al. 2010; Genzel et al. 2010); see Figure 4.

Based on the derived CO(1–0) luminosities, we estimate that the quasar host galaxies contain a molecular gas mass of $(2.7 \pm 0.2) \times 10^{10} M_\odot$ (J0305–3150), $(1.0 \pm 0.2) \times 10^{10} M_\odot$ (J0109–3047), and $(1.2 \pm 0.2) \times 10^{10} M_\odot$ (J2348–3054, see Table 1). We can compare these gas masses with the dynamical mass derived from the [C II] emission line for these quasar host galaxies in Venemans et al. (2016). For J0109–3047 and

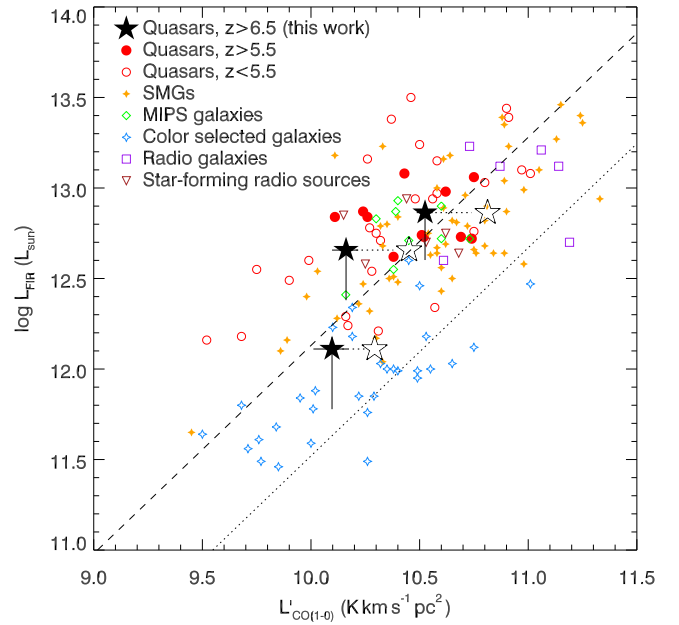


Figure 4. FIR luminosity as function of $L'_{\text{CO}(1-0)}$ for various types of objects at $z > 1$ (adapted from Carilli & Walter 2013). The small, colored symbols are sources with a CO detection at $z > 1$, compiled by Carilli & Walter (2013). Plotted are CO and FIR luminosities of star-forming radio sources (upside-down triangles), radio galaxies (squares), color-selected galaxies at $z > 1$ (small open stars), MIPS 24 μm -selected galaxies (diamonds), sub-millimeter galaxies (SMGs, small filled stars), quasars at $z < 5.5$ (open circles), and quasars at $5.5 < z < 6.5$ (filled circles). Our detections of the $z > 6.5$ quasar hosts are plotted as large, filled stars. The uncertainties in $L'_{\text{CO}(1-0)}$ only reflect the measurement errors and do not include the uncertainty in the CO SLED. This is illustrated by the large, open stars that show the derived $L'_{\text{CO}(1-0)}$ luminosities assuming a different CO excitation ladder (see Section 4.2 for details). The dashed (dotted) line indicates the relation between L_{FIR} and $L'_{\text{CO}(1-0)}$ derived for starburst (star-forming) galaxies up to $z \sim 3.5$ from, e.g., Daddi et al. (2010) and Genzel et al. (2010).

J2348–3054 the dynamical masses are $(1.4 \pm 0.4) \times 10^{11} M_\odot$ and $(7.2 \pm 3.6) \times 10^{10} M_\odot$, and roughly 4%–39% of that dynamical mass is comprised of molecular gas. Assuming dark matter does not significantly contribute to the mass in the center of these galaxies (e.g., Genzel et al. 2017), this suggests that these host galaxies contain a large stellar mass of (at most) $M_* \approx M_{\text{dyn}} - M_{\text{H}_2} = (2-17) \times 10^{10} M_\odot$, which is at the high end of the stellar mass function derived for star-forming galaxies at similar redshifts (e.g., Bowler et al. 2014; Grazian et al. 2015; Stefanon et al. 2015). On the other hand, in J0305–3150, as much as 54%–81% of the dynamical mass of $M_{\text{dyn}} = (4.1 \pm 0.5) \times 10^{10} M_\odot$ comprises molecular gas, which implies a smaller stellar mass of $M_* \lesssim (0.7-2.1) \times 10^{10} M_\odot$. However, the large uncertainties in the derived molecular gas mass and in the dynamical mass prevent us from putting tight constraints on the stellar mass in these quasar hosts.

It should be noted that the uncertainties quoted in this section only include the uncertainties in the measured high- J CO line fluxes and not the uncertainty in the shape of the CO excitation ladder. For example, if we adopt the observed CO SLED of quasars for which high- J and low- J CO lines have been measured from Carilli & Walter (2013), who find luminosity ratios of $L'_{\text{CO}(6-5)}/L'_{\text{CO}(1-0)} \approx 0.34$ and $L'_{\text{CO}(7-6)}/L'_{\text{CO}(1-0)} \approx 0.38$, then the estimated CO(1–0) luminosities (and molecular gas masses) are 57%–95% higher compared to the luminosities derived using the J1148+5251 CO SLED (see Figure 4). A

future measurement of a low- J CO line with the Jansky Very Large Array is essential to obtain a more accurate estimate of the CO(1–0) luminosity in our quasar hosts.

We can verify our CO-based molecular gas mass by computing the gas mass from the amount of dust in the host galaxies presented in Venemans et al. (2016). The quasar hosts have estimated dust masses of $M_d(\text{J0305} - 3150) = (4.5 - 24) \times 10^8 M_\odot$, $M_d(\text{J0109} - 3047) = (0.7 - 4.9) \times 10^8 M_\odot$, and $M_d(\text{J2348} - 3054) = (2.7 - 15) \times 10^8 M_\odot$, which we can use to derive gas masses by assuming local gas-to-dust mass ratios of 70–100 (e.g., Draine et al. 2007; Sandstrom et al. 2013). Similar gas-to-dust mass ratios of ~ 70 have also been found in starburst systems at high redshift (e.g., Riechers et al. 2013; Wang et al. 2016). Using the local gas-to-dust mass ratio, we obtain (atomic and molecular) gas masses of $(3.2 - 24) \times 10^{10} M_\odot$, $(0.5 - 4.9) \times 10^{10} M_\odot$, and $(1.9 - 15) \times 10^{10} M_\odot$, for J0305–3150, J0109–3047, and J2348–3054, respectively. If we further assume that $\sim 75\%$ of the dust-derived gas mass is molecular (e.g., Riechers et al. 2013; Wang et al. 2016), then for J0305–3150 and J0109–3047, the lower values of the dust-derived gas mass agree with the CO-based molecular gas mass. For J2348–3054 the dust mass predicts a higher gas mass.

4.3. Atomic Carbon Mass

We can make use of the [C I] line luminosity (or limits thereof) to calculate the mass of atomic carbon in the quasar host galaxies. If we assume that the [C I] emission is optically thin, then we can use the relation between [C I] brightness and the mass in neutral carbon given by Weiß et al. (2003, 2005):

$$M_{\text{CI}} / M_\odot = 4.566 \times 10^{-4} Q(T_{\text{ex}}) \frac{1}{5} e^{T_2/T_{\text{ex}}} L'_{\text{[C I]}}, \quad (3)$$

where $Q(T_{\text{ex}}) = 1 + 3e^{-T_1/T_{\text{ex}}} + 5e^{-T_2/T_{\text{ex}}}$ is the CI partition function and $T_1 = 23.6$ K and $T_2 = 62.5$ K are the energies above the ground state. Following the literature, we set the excitation temperature to $T_{\text{ex}} = 30$ K (see, e.g. Walter et al. 2011). Note that if we assumed a higher excitation temperature of $T_{\text{ex}} = 50$ K, the derived M_{CI} would be $\sim 38\%$ lower.

For the host galaxy of J2348–3054, in which we tentatively detect the [C I] emission line, we derive a neutral carbon mass of $M_{\text{CI}} = (1.0 \pm 0.4) \times 10^7 M_\odot$. The atomic carbon abundance relative to H₂ is given by $X[\text{C I}] = M_{\text{CI}} / (6M_{\text{H}_2})$. For a sample of $z = 2 - 3$, FIR-bright sources, Walter et al. (2011) derived a carbon abundance of $X[\text{C I}] = (8.4 \pm 3.5) \times 10^{-5}$. Applying this abundance we obtain an independent molecular gas mass in J2348–3054 of $M_{\text{H}_2} = (1.4 - 3.4) \times 10^{10} M_\odot$, which is consistent with the molecular gas mass of $(1.2 \pm 0.2) \times 10^{10} M_\odot$ derived from the CO observations in Section 4.2.

For the other two sources, J0109–3047 and J0305–3150, we can only obtain 3σ upper limits of $M_{\text{CI}} < 9.6 \times 10^6 M_\odot$ and $M_{\text{CI}} < 2.1 \times 10^7 M_\odot$ (Table 1). The upper limits we obtain for the molecular gas mass assuming the neutral carbon abundance from Walter et al. (2011) of $M_{\text{H}_2} < 3 \times 10^{10} M_\odot$ (J0109–3047) and $M_{\text{H}_2} < 7 \times 10^{10} M_\odot$ (J0305–3150) agree well with our molecular gas masses inferred from the CO luminosities.

4.4. The Characteristics of the ISM

With the detection of various FIR lines in our quasar host galaxies, we can start to constrain the physical properties of

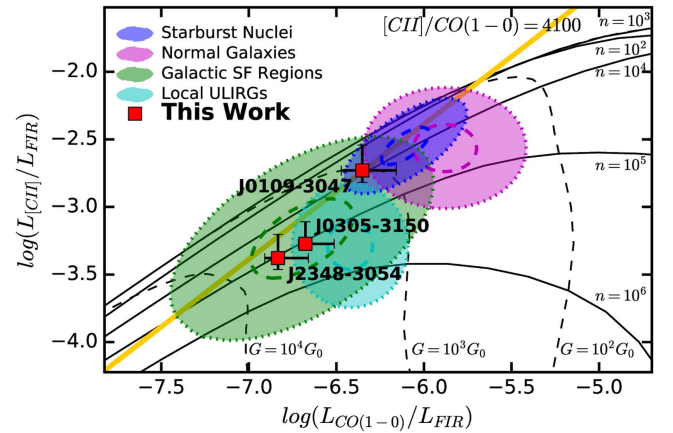


Figure 5. $L_{\text{[C II]}} / L_{\text{FIR}}$ as a function of $L_{\text{CO(1-0)}} / L_{\text{FIR}}$, adapted from Ferkinhoff et al. (2014). Overplotted are values for the UV radiation field G_0 and gas density n from the PDR model of Kaufman et al. (2006). The regions in $L_{\text{[C II]}} / L_{\text{FIR}}$ and $L_{\text{CO(1-0)}} / L_{\text{FIR}}$ occupied by starburst nuclei, normal galaxies, galactic star-forming regions, and local ULIRGs are outlined with colored ellipticals. The values derived for the three $z > 6.6$ quasar hosts are plotted with red squares.

the ISM in these high-redshift galaxies by comparing the luminosity of the emission lines with each other and with the continuum. The observed lines can arise due to star formation in photodissociation regions (PDRs) where the radiation field is dominated by UV photons from young stars, or in X-ray-dominated regions (XDRs), where the X-ray radiation from the accreting black hole dominates the emission (or a combination thereof). Alternatively, a substantial fraction of the [C II] emission could be associated with the diffuse ionized medium. However, observations of local starburst galaxies suggest that only up to 30% of the [C II] emission could be emitted by the diffuse ionized medium (e.g., Carral et al. 1994; Lord et al. 1996; Colbert et al. 1999). Similarly, studies of high-redshift, FIR-luminous sources have concluded that, based on high observed [C II]/[N II] line ratios, at most a small fraction of the [C II] emission comes from the ionized phase of the gas (e.g., Decarli et al. 2014; Pavesi et al. 2016). In the remainder of this section, we will assume that the majority of the [C II] emission comes from the same region as the CO and [C I] emission.

An initial diagnostic plot to test the nature of the emission in our sources is shown in Figure 5, where we plot the luminosity ratio [C II]/FIR as a function of CO(1–0)/FIR. Regions occupied by different galaxies in the nearby universe are shown as well as the typical [C II]/CO(1–0) ratio of $L_{\text{[C II]}} / L_{\text{CO(1-0)}} = 4100$ (Section 4.2). Additionally, contours for UV field strength and gas density are shown for PDR models from Kaufman et al. (1999). These contours show the phase space where PDRs can describe the observed emission line ratios. Sources falling to the upper left, above the typical [C II]/CO(1–0) ratio of 4100, would require a non-PDR emission mechanism such as XDRs to explain the observed lines and continuum. All three of our quasar host galaxies fall in the phase space that can be described by PDRs and are similar to local starbursts and ULIRGs.

The results from the diagnostic shown in Figure 5 can be confirmed, and ISM properties can be derived by applying the PDR and XDR models from Meijerink & Spaans (2005) and

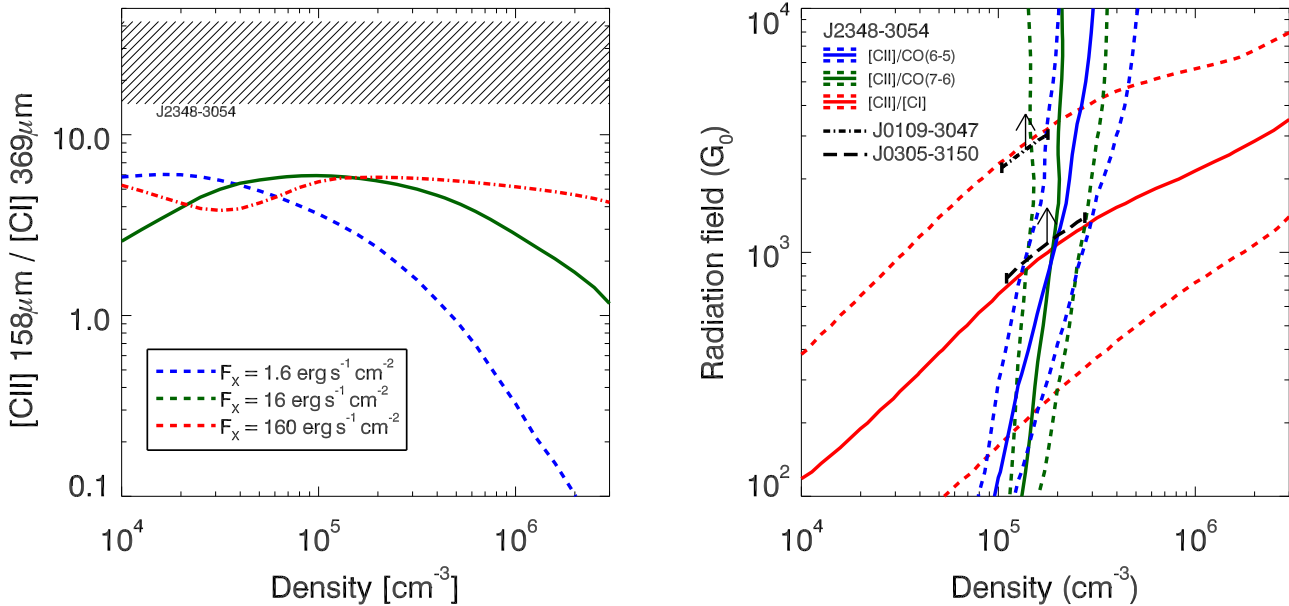


Figure 6. Emission line ratio predictions from the XDR (left) and PDR (right) models of Meijerink et al. (2007). On the left, we plot the [C II]/[C I] luminosity ratio as a function of density for three different values of the X-ray flux. The [C II]/[C I] line ratio never exceeds a value of about 6 in the XDR models. Based on (the limits on) the line ratios of 24^{+19}_{-9} (hashed region), >32 , and >24 that we measure for J2348–3054, J0109–3047, and J0305–3150, respectively, we can exclude the radiation field in these quasar host galaxies as being dominated by the X-ray radiation of the AGN. On the right, we show the constraints on the density and the UV radiation field in the three quasar host galaxies. The red, blue, and green lines show the [C II]/[C I], [C II]/CO(6–5), and [C II]/CO(7–6) line ratios measured in J2348–3054, with the dashed lines indicating the 1σ uncertainty in the line ratios. The dotted-dashed and long-dashed lines show the range of densities and the lower limit on the radiation field for J0109–3047 and J0305–3150, respectively.

Meijerink et al. (2007). In these models the [C II]/CO(7–6) and [C II]/CO(6–5) line ratios range from <1 to >300 , depending on the density and radiation field (UV radiation in the case of a PDR and X-ray radiation for XDR models). In contrast, the [C II]/[C I] line ratio is predicted to be significantly different for a PDR and an XDR. While for a PDR the [C II]/[C I] ratio is anticipated to lie between ~ 3 –50, the range is predicted to be $\lesssim 6$ for XDRs; see Figure 6. We can compare this range with the values measured in our quasar host galaxies. For J2348–3054, we derive a ratio of $[C\text{ II}]/[C\text{ I}] \approx 24$, while for J0109–3047 and J0305–3150, the non-detection of the [C I] line results in lower limits of >32 and >24 , respectively. All these values are significantly higher than the maximum line ratio predicted for XDRs in the models of Meijerink et al. (2007). Based on these models we conclude that the heating of the ISM is dominated by star-formation.

In contrast to the results shown in Figure 5, for J2348–3054 (for which we measured the strength of the [C II] CO(6–5), CO(7–6), and [C I] lines) we can constrain the density and radiation field without relying on assumptions on the shape of the FIR emission and the CO excitation ladder. The results are shown in Figure 6. From the various line ratios, we derive a density of $\sim 2 \times 10^5 \text{ cm}^{-3}$ and a radiation field strength of $\sim 10^3 G_0$, with G_0 being the radiation field strength in Habing units, $1.6 \times 10^3 \text{ erg s}^{-1} \text{ cm}^{-2}$. Also shown in Figure 6 are the constraints on the ISM properties in J0109–3047 and J0305–3150. From the [C II]-to-CO line ratios we obtain densities of $n_{J0109-3047} \approx 10^5 \text{ cm}^{-3}$ and $n_{J0305-3150} \approx 2 \times 10^5 \text{ cm}^{-3}$. The non-detection of the [C I] line results in a lower limit on the radiation field strength of $G_{J0109-3047} > 2 \times 10^3 G_0$ and $G_{J0305-3150} > 10^3 G_0$.

If we assume that the [C II] flux coming from the PDR is only a factor 0.7 of the observed value (as found in local starbursts; see the discussion above), then from the PDR

models we derive for J2348–3054 a slightly higher density of $2.3 \times 10^5 \text{ cm}^{-3}$ and a lower radiation field strength of $5 \times 10^2 G_0$. To further constrain the properties of the ISM in these quasar host galaxies, observations of additional FIR emission lines are required.

With the derived values for the density and the radiation field from the PDR models, we can compare the properties of the ISM in the VIKING quasar hosts with those in other $z > 6$ sources. The host galaxies of the quasar J1148+5251 at $z = 6.42$ have been detected in many emission lines, including [C II] (e.g., Maiolino et al. 2005; Walter et al. 2009), CO (e.g., Bertoldi et al. 2003b; Walter et al. 2003; Riechers et al. 2013; Stefanon et al. 2015), and [C I] (Riechers et al. 2009). The [C II]/CO(7–6) ratio is very similar to that of the VIKING quasar hosts, suggesting that the ISM density is also around $2 \times 10^5 \text{ cm}^{-3}$. On the other hand, the [C II]/[C I] ratio in J1148+5251, $L_{[\text{C II}]} / L_{[\text{C I}]} \approx 42$ (Riechers et al. 2013), is higher than what we measured in J2348–3054. Based on the PDR models of Meijerink & Spaans (2005, Figure 6), this would require a radiation field strength of $\sim 4 \times 10^3 G_0$. Wang et al. (2016) found very comparable values for the density and radiation field in the host of quasar J0100+2802 at $z = 6.3$ based on the strength of the [C II] CO(6–5), and CO(2–1) emission lines and the FIR luminosity: $n = 1 \times 10^5 \text{ cm}^{-3}$ and $G = 4 \times 10^3 G_0$. Although both the quasar luminosity and the derived values for G are higher for J1148+5251 and J0100+2802 compared to the VIKING quasars and may point to a relation between the quasar luminosity and G , there is no evidence for such a relation among our VIKING sources: the faintest quasar in our sample is J0109–3047, both in quasar luminosity (Venemans et al. 2013) and in FIR luminosity (Venemans et al. 2016), and has the highest (limit on) G . This is confirmed when analyzing the emission line ratios in the starburst HFLS3 at $z = 6.34$ (Riechers et al. 2013), a very massive galaxy without a

luminous AGN. Again, the [C II]/CO(7–6) ratio in HFLS3 is very similar to those in the $z > 6.5$ quasar hosts, while the [C II]/[C I] line ratio is >51 , which implies a very high radiation field (Figure 6).

5. Summary

In this paper, we present ALMA band 3 observations of the CO(6–5), CO(7–6), and [C I] $369\text{ }\mu\text{m}$ emission lines in three of the highest-redshift quasar host galaxies at $6.6 < z < 6.9$. The sample has been previously detected in [C II] $158\text{ }\mu\text{m}$ emission and the underlying FIR dust continuum (Venemans et al. 2016). CO is detected at high significance in all sources, making these measurements the highest-redshift CO detections to date. Given the resolution of our observations ($\gtrsim 2''.5$, or $>12\text{ kpc}$), all quasar hosts are spatially unresolved in the current data.

In two of our sources, we detect the continuum emission around the CO emission lines (around $400\text{ }\mu\text{m}$ rest-frame). A comparison with the previously measured dust continuum at higher frequencies (close to the [C II] line) gives dust temperatures that are broadly consistent with the canonical value of 47 K, albeit the current uncertainties are very large. Future observations of multi-frequency continuum emission clearly have the potential to derive more accurate dust temperatures, and possibly spatially resolved temperature gradients.

Assuming a CO SLED similar to that observed in the $z = 6.4$ quasar J1148+5251, we derive molecular gas reservoirs of $1\text{--}3 \times 10^{10} M_\odot$ in the quasar hosts. For J2348–3054 and J0109–3047, we estimate high stellar masses of $M_* = (2\text{--}17) \times 10^{10} M_\odot$. For J0305–3150, as much as $\sim 54\text{--}81\%$ of the dynamical mass is in the form of molecular gas, indicating that the stellar mass is $M_* < 2.1 \times 10^{10} M_\odot$, less than $22\times$ the mass of the central black hole ($M_{\text{BH}} = 9.5 \times 10^8 M_\odot$; De Rosa et al. 2014). We possibly overestimated the molecular gas mass in this quasar host (if, for example, the CO(6–5)/CO(1–0) and CO(7–6)/CO(1–0) luminosity ratios are larger in J0305–3150 than that measured in J1148+5251), or the dynamical mass is significantly larger than the mass traced by the [C II] emission. The extrapolated [C II]-to-CO(1–0) luminosity ratio is 2500–4200, consistent with measurements in galaxies at lower redshift.

The (marginal) detection of [C I] emission in one quasar host galaxy (at $z = 6.9$) and the limit on the [C I] emission in the other two galaxies enables us to characterize the physical properties of the ISM in $z \sim 7$ quasar hosts for the first time. In this case, the derived global CO/[C II]/[C I] line ratios are consistent with them emerging from PDRs, but inconsistent with an excitation from XDRs. This implies that if the central supermassive black hole gives rise to an XDR, it does not dominate the excitation of the overall gas reservoir. This finding provides further evidence that the quasar host galaxies studied in this paper harbor intense starbursts, and provides justification to link quantities derived for the molecular gas and dust content to ongoing star formation in these quasar hosts.

The observations presented here represent only a modest investment of ALMA time (with typical on-source integration times between 15 and 35 minutes). This implies that future observations have the potential to resolve the molecular gas emission, which eventually could lead to spatially resolved excitation measurements within the quasar host galaxies at the highest redshift. Furthermore, by targeting other FIR emission

lines, such as [O I] $146\text{ }\mu\text{m}$, [N II] $122\text{ }\mu\text{m}$, and [O III] $88\text{ }\mu\text{m}$, we will be able to put additional constraints on the properties and metallicity of the ISM in these forming massive galaxies in the early universe.

We thank the referee for providing comments that helped to improve the manuscript. B.P.V. and F.W. acknowledge funding through the ERC grant “Cosmic Dawn.” Support for R.D. was provided by the DFG priority program 1573 “The physics of the interstellar medium.” R.G.M. acknowledges the support of the UK Science and Technology Facility Council (STFC). This paper makes use of the following ALMA data: ADS/JAO.ALMA#2013.1.00273.S. ALMA is a partnership of ESO (representing its member states), NSF (USA), and NINS (Japan), together with NRC (Canada), and NSC and ASIAA (Taiwan), in cooperation with the Republic of Chile. The Joint ALMA Observatory is operated by ESO, AUI/NRAO, and NAOJ.

Facility: ALMA.

ORCID iDs

- Bram P. Venemans <https://orcid.org/0000-0001-9024-8322>
 Fabian Walter <https://orcid.org/0000-0003-4793-7880>
 Roberto Decarli <https://orcid.org/0000-0002-2662-8803>
 Carl Ferkhoff <https://orcid.org/0000-0001-6266-0213>
 Axel Weiß <https://orcid.org/0000-0003-4678-3939>
 Richard G. McMahon <https://orcid.org/0000-0001-8447-8869>

References

- Bañados, E., Decarli, R., Walter, F., et al. 2015, *ApJL*, 805, L8
 Bañados, E., Venemans, B. P., Decarli, R., et al. 2016, *ApJS*, 227, 11
 Beelen, A., Cox, P., Benford, D. J., et al. 2006, *ApJ*, 642, 694
 Bertoldi, F., Carilli, C. L., Cox, P., et al. 2003a, *A&A*, 406, L55
 Bertoldi, F., Cox, P., Neri, R., et al. 2003b, *A&A*, 409, L47
 Bowler, R. A. A., Dunlop, J. S., McLure, R. J., et al. 2014, *MNRAS*, 440, 2810
 Carilli, C. L., Neri, R., Wang, R., et al. 2007, *ApJL*, 666, L9
 Carilli, C. L., & Walter, F. 2013, *ARA&A*, 51, 105
 Carral, P., Hollenbach, D. J., Lord, S. D., et al. 1994, *ApJ*, 423, 223
 Colbert, J. W., Malkan, M. A., Clegg, P. E., et al. 1999, *ApJ*, 511, 721
 da Cunha, E., Groves, B., Walter, F., et al. 2013, *ApJ*, 766, 13
 Daddi, E., Bournaud, F., Walter, F., et al. 2010, *ApJ*, 713, 686
 De Rosa, G., Decarli, R., Walter, F., et al. 2011, *ApJ*, 739, 56
 De Rosa, G., Venemans, B. P., Decarli, R., et al. 2014, *ApJ*, 790, 145
 Decarli, R., Walter, F., Carilli, C., et al. 2014, *ApJL*, 782, L17
 Decarli, R., Walter, F., Venemans, B. P., et al. 2017, *Natur*, 545, 457
 Downes, D., & Solomon, P. M. 1998, *ApJ*, 507, 615
 Draine, B. T., Dale, D. A., Bendo, G., et al. 2007, *ApJ*, 663, 866
 Fan, X., Strauss, M. A., Becker, R. H., et al. 2006, *AJ*, 132, 117
 Ferkhoff, C., Brisbin, D., Parshley, S., et al. 2014, *ApJ*, 780, 142
 Gallerani, S., Ferrara, A., Neri, R., & Maiolino, R. 2014, *MNRAS*, 445, 2848
 Genzel, R., Schreiber, N. M. F., Übler, H., et al. 2017, *Natur*, 543, 397
 Genzel, R., Tacconi, L. J., Graciá-Carpio, J., et al. 2010, *MNRAS*, 407, 2091
 Grazian, A., Fontana, A., Santini, P., et al. 2015, *A&A*, 575, A96
 Gullberg, B., De Breuck, C., Vieira, J. D., et al. 2015, *MNRAS*, 449, 2883
 Jiang, L., Fan, X., Vestergaard, M., et al. 2007, *AJ*, 134, 1150
 Kaufman, M. J., Wolfire, M. G., & Hollenbach, D. J. 2006, *ApJ*, 644, 283
 Kaufman, M. J., Wolfire, M. G., Hollenbach, D. J., & Luhman, M. L. 1999, *ApJ*, 527, 795
 Kurk, J. D., Walter, F., Fan, X., et al. 2007, *ApJ*, 669, 32
 Leipski, C., Meisenheimer, K., Walter, F., et al. 2014, *ApJ*, 785, 154
 Lord, S. D., Hollenbach, D. J., Haas, M. R., et al. 1996, *ApJ*, 465, 703
 Maiolino, R., Cox, P., Caselli, P., et al. 2005, *A&A*, 440, L51
 Matsuoka, Y., Onoue, M., Kashikawa, N., et al. 2016, *ApJ*, 828, 26
 Mazzucchelli, C., Bañados, E., Venemans, B. P., et al. 2017, *ApJ*, submitted
 McMullin, J. P., Waters, B., Schiebel, D., Young, W., & Golap, K. 2007, in *ASP Conf. Ser.* 376, *Astronomical Data Analysis Software and Systems XVI*, ed. R. A. Shaw, F. Hill, & D. J. Bell (San Francisco, CA: ASP), 127

- Meijerink, R., & Spaans, M. 2005, *A&A*, **436**, 397
- Meijerink, R., Spaans, M., & Israel, F. P. 2007, *A&A*, **461**, 793
- Mortlock, D. J., Warren, S. J., Venemans, B. P., et al. 2011, *Natur*, **474**, 616
- Pavesi, R., Riechers, D. A., Capak, P. L., et al. 2016, *ApJ*, **832**, 151
- Priddey, R. S., & McMahon, R. G. 2001, *MNRAS*, **324**, L17
- Riechers, D. A., Bradford, C. M., Clements, D. L., et al. 2013, *Natur*, **496**, 329
- Riechers, D. A., Walter, F., Bertoldi, F., et al. 2009, *ApJ*, **703**, 1338
- Sandstrom, K. M., Leroy, A. K., Walter, F., et al. 2013, *ApJ*, **777**, 5
- Stacey, G. J., Geis, N., Genzel, R., et al. 1991, *ApJ*, **373**, 423
- Stefan, I. I., Carilli, C. L., Wagg, J., et al. 2015, *MNRAS*, **451**, 1713
- Stefanon, M., Marchesini, D., Muzzin, A., et al. 2015, *ApJ*, **803**, 11
- Venemans, B. P., Bañados, E., Decarli, R., et al. 2015, *ApJL*, **801**, L11
- Venemans, B. P., Findlay, J. R., Sutherland, W. J., et al. 2013, *ApJ*, **779**, 24
- Venemans, B. P., McMahon, R. G., Walter, F., et al. 2012, *ApJL*, **751**, L25
- Venemans, B. P., Walter, F., Decarli, R., et al. 2017, *ApJ*, **837**, 146
- Venemans, B. P., Walter, F., Zschaechner, L., et al. 2016, *ApJ*, **816**, 37
- Walter, F., Bertoldi, F., Carilli, C., et al. 2003, *Natur*, **424**, 406
- Walter, F., Riechers, D., Cox, P., et al. 2009, *Natur*, **457**, 699
- Walter, F., Weiβ, A., Downes, D., Decarli, R., & Henkel, C. 2011, *ApJ*, **730**, 18
- Wang, R., Carilli, C. L., Beelen, A., et al. 2007, *AJ*, **134**, 617
- Wang, R., Carilli, C. L., Neri, R., et al. 2010, *ApJ*, **714**, 699
- Wang, R., Carilli, C. L., Wagg, J., et al. 2008, *ApJ*, **687**, 848
- Wang, R., Wagg, J., Carilli, C. L., et al. 2011a, *ApJL*, **739**, L34
- Wang, R., Wagg, J., Carilli, C. L., et al. 2011b, *AJ*, **142**, 101
- Wang, R., Wagg, J., Carilli, C. L., et al. 2013, *ApJ*, **773**, 44
- Wang, R., Wu, X.-B., Neri, R., et al. 2016, *ApJ*, **830**, 53
- Weiβ, A., Downes, D., Henkel, C., & Walter, F. 2005, *A&A*, **429**, L25
- Weiβ, A., Henkel, C., Downes, D., & Walter, F. 2003, *A&A*, **409**, L41
- Willott, C. J., Bergeron, J., & Omont, A. 2015, *ApJ*, **801**, 123
- Willott, C. J., Omont, A., & Bergeron, J. 2013, *ApJ*, **770**, 13
- Wu, X.-B., Wang, F., Fan, X., et al. 2015, *Natur*, **518**, 512